Warm Dark Matter Galaxy Formation

RACHEL KENNEDY

WARM DARK MATTER GALAXY FORMATION

Rachel Kennedy

A Thesis presented for the degree of
MSc

Insitute for Computational Cosmology
Department of Physics
University of Durham
England

September 2014

Warm Dark Matter Galaxy Formation

Rachel Kennedy

Submitted for the degree of MSc

September 2014

Abstract

Numerous hypothetical particles have been predicted which might possibly make up the dark matter content of the Universe. One class of these particle candidates includes warm dark matter (WDM) particles, which have large early-time thermal velocities that serve to erase small-scale perturbations. This creates a cutoff in the linear power spectrum - the scale of which depends on the mass of the WDM particle - and results in a suppression in the numbers of low mass halos. Since the number of satellite galaxies around Milky Way-mass host galaxies is sensitive to this cutoff, we can use the number of satellites actually observed around our own galaxy as a test of different WDM models (such as sterile neutrinos).

First, we explore the simplest case of a thermal relic WDM particle (and alternatively a sterile neutrino produced via non-resonant oscillations). We use the GALFORM semi-analytic model of galaxy formation to compare predicted satellite luminosity functions to Milky Way data and determine a lower bound on the WDM particle mass. This depends strongly on the Milky Way halo mass, and to some extent, on the baryonic physics assumed. For our fiducial model we find that for a thermal relic particle mass of 3.3 keV (the 2σ lower limit from an analysis of the Lyman-α forest by Viel et al.) the Milky Way halo mass is required to be $> 1.4 \times 10^{12}$ $M_{\odot}$. For this same fiducial model, we also find that all WDM particle masses are ruled out (at 95% confidence) if the Milky Way halo mass is smaller than 1.0×10^{12} $M_{\odot}$, while if the mass of the Galactic halo is less than 1.8 $\times 10^{12}$ $M_{\odot}$, only WDM relic particle masses larger than 2 keV are allowed.

Next, we consider models in which some of the WDM particles are resonantly produced sterile neutrinos, which behave "colder" than the non-resonantly produced population also being generated. This model of sterile neutrino dark

matter is well-motivated theoretically, and is also in less conflict with current Lyman-α bounds. This scenario then becomes a two-parameter problem involving both the particle mass and the resonant fraction. We repeat the satellite abundance test applied to this new problem to rule out parts of the parameter space for different Milky Way halo masses. Focusing on a 7 keV sterile neutrino particle which may have been hinted at by recent observations, we find that if the Milky Way halo mass is 2×10^{12} $M_\odot$ then most cases are allowed, but if the mass is 1×10^{12} $M_\odot$ then this particle is likely ruled out.

Warm Dark Matter Galaxy Formation

Rachel Kennedy

A Thesis presented for the degree of
MSc

Insitute for Computational Cosmology
Department of Physics
University of Durham
England

September 2014

CONTENTS

DECLARATION

The work described in this thesis was undertaken between 2011 and 2014 while the author was a research student under the supervision of Professor Shaun Cole and Professor Carlos Frenk at the Institute for Computational Cosmology, the Department of Physics, Durham University, England. No part of this thesis has been submitted elsewhere for any other degree or qualification and it is all my own work unless referenced to the contrary in the text.

Chapter 2 of this thesis has been published in the form of a paper,

- Kennedy R., Frenk C., Cole S., Benson A., *"Constraining the WDM Particle Mass with Milky Way Satellites"*, 2014, MNRAS, 442 (3)

ACKNOWLEDGEMENTS

First and foremost, I would like to express my gratitude to my supervisors Carlos Frenk and Shaun Cole, for their phenomenal support, guidance and mentorship. Thank you so much for all your help with projects, your insights and ideas, and for being so warm and welcoming into Durham, and into the department.

Everyone at the ICC in Durham has been so helpful, and I want to give special thanks to John Helly and Lydia Heck for answering my numerous questions and assisting me with many quandaries. My collaborators within and outside the department have been incredibly helpful and resourceful, especially Mark Lovell -this work would not have been possible without all of them.

The friends I've met during my time here are a fantastic group, and while there are too many to name here, I want to express how hugely appreciative I am for their support and companionship. The people I've shared offices with, houses with and coffee with have been a pleasure to come to know over these couple years.

The calculations performed for this work were carried out on the Cosmology Machine supercomputer at the Institute for Computational Cosmology, Durham. The Cosmology Machine is part of the DiRAC Facility jointly funded by STFC, the Large Facilities Capital Fund of BIS, and Durham University. This work was supported in part by the STFC rolling grant ST/F001166/1 to the ICC and by the National Science Foundation under Grant No. PHYS-1066293.

1 INTRODUCTION

Since the 1930s, the astrophysical evidence of the existence of dark matter has been mounting, supported by measurements of clustering, galaxy rotation curves, lensing and CMB fluctuations. The most recent Planck satellite data release puts the matter density of the universe at $\Omega_{\mathrm{m}} = 0.32$, of which roughly 82% is non-baryonic "dark" matter. The nature of this substance is largely unknown. Predictions from particle physics about the existence of several hypothetical particles prompt us to consider some of these as potential candidates for the unknown dark matter particle.

1.1 Cold and Warm Dark Matter

In the standard cosmological model, the dark matter is a cold particle, but we can also look at different possible temperatures of dark matter, and what the resulting effects on structure formation would look like (see Frenk & White, 2012 for a review). Though the boundaries between "cold", "warm" and "hot" dark matter are somewhat fluid, we can divide them into general categories based upon their characteristics. Cold dark matter (CDM), the most popular model, decouples while non-relativistic, and any free-streaming of the particles is negligible. For relativistic hot dark matter particles, which have been ruled out as the main dark matter particle, free-streaming erases structures below cluster scales. Warm dark matter (WDM) is an intermediate case: free-streaming is an important effect at early times in washing out small perturbations, but particles are

"cold" today. This scenario leads to a cutoff in the linear power spectrum which varies with the mass and production mechanism of the WDM particle; the smallest collapsed halos are roughly dwarf-galaxy size. Well-motivated hypothetical CDM candidates include the axion and the neutralino. Some plausible WDM candidates are the sterile neutrino (e.g. Dodelson & Widrow, 1994; Shi & Fuller, 1999; Asaka & Shaposhnikov, 2005; see Kusenko, 2009 for a review) and gravitino (Pagels & Primack, 1982; Moroi et al., 1993; Gorbunov et al., 2008).

In the future, the identity of the dark matter may be revealed through direct detection experiments, or by indirect detection of an annihilation signal. A report of a 130 GeV line observed near the MW centre (Weniger, 2012) has been interpreted as a possible sign of dark matter annihilation occurring there, although this result is still inconclusive. In the meantime, one of the most promising ways we have of learning more about the identity of the dark matter is via its imprint on the development of structure in the universe.

On large scales CDM and WDM models predict a similar evolution of structure, so the critical scales at which to differentiate the models will be around or below the WDM cutoff wavelength. In the standard CDM model, where free-streaming is unimportant, halos are expected to form down to around an Earth-mass, with a halo mass function that continues to increase with decreasing mass (e.g. Jenkins et al., 2001; Tinker et al., 2008; Diemand et al., 2007; Springel et al., 2008). On large scales, the CDM model predictions are well-tested by CMB and clustering measurements: any successful cosmological model for dark matter is constrained to also account for these observations.

On small scales, WDM models have an overall reduction of power, with a cutoff wavelength which shifts to larger scales as the particle mass decreases. This cutoff can take the form of a simple truncation of all power below some cutoff, or have a more complex multi-component form depending on the specific model of particle production. The net effect of this suppression is a reduction in the number of low-mass halos, typically tapering off around the mass of a dwarf galaxy. Halos of the same mass collapse later in WDM, when the background density of the universe is lower. As a result, halos of the same mass will have

lower concentrations in WDM compared to CDM, and concentrations additionally decrease with decreasing $m_{\rm WDM}$ (Avila-Reese et al., 2001; Lovell et al., 2012, 2014; Schneider et al., 2012). This has repercussions for the efficacy of feedback processes in their hosted galaxies, as well as how easily these systems can be tidally disrupted during mergers.

The dependence of the cutoff on the mass and other characteristics of the WDM particle, means that we can use predictions about subgalactic structure in different models in order to place constraints upon the WDM particle mass.

1.2 WDM Simulations

Dwarf galaxies are the smallest clumps of dark matter identified so far. The dwarf halos often host satellite galaxies of larger systems, such as the many identified in our own Local Group. They are the most dark matter dominated objects observed, with typical mass-to-light ratios of up to $\sim$100 for the Milky Way satellites. This makes them ideal for understanding the properties of the DM and testing different models.

It has been argued that the Milky Way dwarfs may all have "cored" inner density profiles, where the central density is constant at small radii $r \lesssim 1$ kpc (see de Blok, 2010 for a review). This conclusion is interesting because it appears at odds with the results of CDM simulations, which predict universally cusped inner halo profiles, in which the density continues to increase steeply towards the centre (Navarro et al., 1996, 1997; Springel et al., 2008). This could suggest either a misconception about the nature of the DM as a cold, collisionless particle (e.g. Zavala et al., 2013), or an underestimation of the role of baryons in reshaping halo structure (Pontzen & Governato, 2012). Additionally, the number and distribution of satellite galaxies around MW-mass hosts are further tests of our theories of dark matter. The large abundance of low-mass halos predicted in CDM simulations compared with the relatively fewer number of satellites actually observed was once considered a "missing satellites problem"; this is no longer considered a conflict because it is clear that the combined effects of reion-

ization and supernova feedback in stifling star formation account neatly for this discrepancy of halo and galaxy counts (e.g. Benson et al., 2002b,a; Somerville, 2002). However, another problem arises: CDM simulations imply that the most massive subhalos of $\sim 10^{12}$ $M_\odot$ galaxies are too concentrated to be compatible hosts for the bright MW satellites observed. But it also seems implausible that such large subhalos would preferentially remain dark; this is the so-called "too big to fail" problem identified by Boylan-Kolchin et al. (2011). The solution to this disparity could lie in powerful feedback (Pontzen & Governato, 2012), a lighter-than-expected MW halo mass (Wang et al., 2012; Purcell & Zentner, 2012), or an alternative DM model (Lovell et al., 2012). The radial distribution of dwarfs around larger central galaxies is also a benchmark for different DM theories. For example, it has been noted that the MW dwarfs appear much more radially concentrated than CDM simulation predictions. Some of this apparent tension may be relieved if it turns out that our own galaxy has an unusual dwarf distribution compared to other similar galaxies (Yniguez et al., 2014).

Numerical simulations of the evolution of structure in our universe are an invaluable tool in testing and comparing different cosmological models, as the scales of interest are highly non-linear. The first cosmological simulations in the 1960s featured hundreds of particles; current state-of-the-art simulations now have up to hundreds of billions. Dark matter-only (DMO) simulations are the simplest and most common implementation, exploiting the dominance of dark matter as the main contributor to the matter density of our universe and neglecting the effects of baryons on structure formation altogether. This makes them cheaper to run than hydrodynamical simulations, allowing large-scale and high-resolution tests of the effects of different kinds of dark matter. These DMO simulations can be post-processed with semi-analytic galaxy formation models (e.g. Cole et al., 2000) to predict the formation and evolution of galaxies within the merging dark halos. There are some tensions between simulations and observations, especially on small scales (e.g. cusp/core issue), which may require more detailed treatment of the baryons at the centres of the halos. Still, this approach has been largely successful in producing a distribution and population

of galaxies consistent with observations.

A simulation of hot dark matter (HDM) was performed by White et al. (1983). At the time, neutrinos were a popular dark matter candidate, as they were a "dark" particle that was already known to exist. However, this work demonstrated that the HDM washed out structures below galaxy cluster scales and that neutrinos alone could not account for the observed clustering today. Warm models face similar challenges; the free-streaming scale is smaller than for HDM, but if the particle is too warm, then the model will not produce enough low mass halos, and be in contention with local observations.

Some of the first simulations of WDM structure formation were done by Colín et al. (2000), and by Bode et al. (2001). These studies were motivated by the small-scale "problems" of CDM, such as the seeming overabundance of low-mass CDM subhalos compared with observed Milky Way dwarfs, and the high central concentrations of simulated CDM halos. The conclusion of these analyses was that WDM was successful in producing a similar number of subhalos around MW-mass galaxies as seen around the MW, and also in suppressing the number of void dwarfs to be more on par with observations. However, while WDM halos are less concentrated than their CDM counterparts of the same mass, the authors found that in order to get the sizeable cores argued for by analyses of the MW dwarf data, the WDM particle mass would have to be unrealistically small (see also Macciò et al., 2012; Shao et al., 2013).

One difficulty of these WDM simulations is that they suffer from the problem of spurious fragmentation of low-mass halos, which were initially interpreted as genuine objects instead of a numerical artefact. Wang & White (2007) first identified this issue, finding that at the root of the issue is the excess of power on the scale of the mean interparticle separation, due to the discreteness of the N-body simulation, which was prompting the collapse of these small, regularly-spaced halos forming along filaments. These "spurious" halos can be discerned by tracing the morphology of their member particles back to the initial conditions, using the methods layed out in Lovell et al. (2014). These objects can then be "cleaned" from catalogues when developing halo merger trees (the same mate-

rial is assumed to accrete, but should have been acquired as smooth accretion instead of discrete lumps). Still, as these spurious mini-halos are endemic to the simulations (though see also Angulo et al., 2013), this artificially lumpy accretion may put limits on the conclusions we might draw regarding what these simulations can tell us about the structure of WDM halos.

The large early-time thermal velocities of WDM particles are usually not represented in simulations, as the implementation of this effect is ambiguous. Typically it is assumed that the bulk of the free streaming effect has already happened by the start of the simulation, which justifies ignoring the thermal velocities altogether. Avila-Reese et al. (2001) performed WDM simulations with and without the incorporation of thermal velocities, and found virtually no differences to the internal structures of the halos when the velocities were included.

The Aquarius Project (Springel et al., 2008) is a suite of six CDM cosmological zoom simulations of galactic halos at high resolution, each with a mass similar to that of the Milky Way. As this figure is somewhat uncertain, these masses range from $M_{200} \sim 8 \times 10^{11} - 1.8 \times 10^{12}$ $M_\odot$. The Aquarius halos were simulated at several different resolution levels, numbered "1" to "5" ($m_p \sim 2 \times 10^3 - 3 \times 10^6$ $M_\odot$, respectively). The highest resolution for which all six Aquarius halos (labelled "A" through "F") have been run is Level 2, which corresponds to $m_p \sim 10^4$ $M_\odot$.

While the original Aquarius project focused on MW-analogue halo properties in a CDM universe, the same halos have also been simulated for some WDM scenarios (e.g. Lovell et al. 2012). The WDM runs currently represent models with thermal relic particle masses ranging from 1.5 to 2.3 keV, and a further set of models including some C+WDM tests are being carried out. This allows for direct comparisons to be made between the unfolding of events in the different models. Many of the larger subhalos have directly identifiable counterparts between CDM and WDM, which provides insight into how merging events and halo morphology might be affected by the changes to the power spectrum. Lovell et al. (2014) used the subhalo counts from the warm Aquarius simulations to put lower limits on the WDM particle mass, similar to the approach we will

take here using Monte Carlo methods. Here, we will make use of these simulations to examine how the presence of WDM would affect predictions about the formation of the MW stellar halo via tidal disruption of satellite systems as they are accreted onto the main halo.

In order to be able to make more detailed comparisons to the observable universe, we need to link the evolution of these dark matter only simulations to the galaxies which are forming within them. Semi-analytic models of galaxy formation provide this function by using simplified prescriptions for gas cooling, star formation and the mechanics of supernova/AGN feedback within the context of the hierarchically merging halos of the input trees. A number of free parameters representing uncertainties in the galaxy formation process can be adjusted to provide the best fit to the data, including luminosity functions, metal contents, size distribution and other quantities. Although we are primarily interested (here) in the properties of the dwarf galaxies of MW-type systems, it is important to reproduce the behaviour of the overall galaxy population to ensure a good fit. For WDM models these parameters may require re-tuning to account for the later formation and lower concentration of halos. It is also conceivable that some extensions to the galaxy formation model may have to be added, for example if star formation in WDM filaments turns out to be a significant effect (e.g. Gao & Theuns, 2007; Gao et al., 2014).

Here we use the Durham semi-analytic model of galaxy formation, GALFORM. The halo merger trees are constructed using the "Dhalo" algorithm (Jiang et al., 2014) to accurately link structures between snapshots of the simulation.

1.3 Current Status of WDM Models

Hints of a 7 keV sterile neutrino have emerged recently from the work of two groups, released simultaneously. Boyarsky et al. (2014b) and Bulbul et al. (2014) looked at x-ray spectra of Andromeda and the Perseus cluster, and at the spectra of 73 bright clusters, respectively, and independently found an excess 3.5 keV signal. (There has now also been a reported detection in the MW by Boyarsky et al.,

2014a.) Among other possibilities, this emission line could be the result of a 7 keV sterile neutrino decay. Although this conclusion is very tentative, it prompts us to consider with special attention sterile neutrino models around this mass range.

As outlined earlier, the "warm dark matter" label encompasses many different models, motivated by both astrophysical evidence and particle physics theories. The main tenet that unites these models is the curtailment of power on small scales.

Given that the definition of WDM is so broad, there is no clear-cut distinction of where "warm" ends and "cold" begins. As the mass of the proposed particle increases, the astrophysical differences (halo mass function, mass-concentration relation, etc.) between CDM and WDM will diminish until becoming virtually indistinguishable. In this "lukewarm" regime, the specific characteristics of individual dark matter candidates will become increasingly important in terms of discovering more about the identity of the dark matter. Different particles may leave different signatures that we can search for directly or indirectly. For example, sterile neutrinos are predicted to decay into a neutrino and a photon, producing a signal that can be searched for. Furthermore, the predicted production of these x-ray decays might have other consequences as well, such as for the progression of reionization, which can also be analyzed.

In placing lower limits, we are constrained at the low-mass end by the necessity of producing adequate amounts of substructure as is actually observed. For example, we explore in this work the "reverse missing satellites" problem, in which too few dwarf galaxy host subhalos are found around MW-mass central hosts. Similar studies of this nature have been carried out by Lovell et al. (2014) and Polisensky & Ricotti (2011).

Some of the most stringent limits have come from analyses of the Lyman-α flux power spectrum between redshifts $z \sim 2-6$ (when the scales of interest are still mildly non-linear) in conjunction with WDM simulations (e.g. Narayanan et al., 2000; Viel et al., 2005). Using high-resolution hydrodynamical simulations to interpret the small-scale clumpiness of the Lyman-α flux power

spectrum measured from high-resolution spectra of 25 $z > 4$ quasars, Viel et al. (2013) have set a lower limit of $m_{\rm WDM} \geq 3.3$ keV (non-resonant $m_{\rm sterile} \geq 22$ keV) for the warm dark matter particles.

Another method of finding limits is by invoking the need to produce enough ionizing photons at high redshift for reionization to happen by $z \sim 6$, which sets $m_{\rm WDM} \geq 1.3$ keV (Barkana et al., 2001; Schultz et al., 2014). Or alternatively, by demanding that enough structure be present at early enough times to account for some observed high-redshift GRBs, as overviewed in de Souza et al. (2013). The frequency of lensing events of high-redshift supernova has also been proposed as a way of placing constraints (Pandolfi et al., 2014).

Other independent limits may come from confronting observed lensing flux anomalies with WDM models (e.g. Miranda & Macciò, 2007; $m_{\rm WDM} \geq 1.8$ keV), or from the measured central phase space densities of the MW dwarfs, which sets lower bounds of $m_{\rm WDM} \geq 0.5$ keV.

Sterile neutrinos are predicted to be produced via non-resonant oscillations of active neutrinos. In the Dodelson-Widrow (DW; Dodelson & Widrow, 1994) model, this is the sole mode of production. The DW model as the *only* production mechanism of dark matter in the universe has been ruled out: the lack of observed x-rays from M31 place upper limiting bounds upon the allowed mass/mixing angle of the neutrinos. To satisfy this x-ray constraint while still producing the correct abundance of dark matter, the sterile neutrino particle must be less than ~ 4 keV (Boyarsky et al., 2009), which is in conflict with Lyman-α bounds.

In addition to this non-resonant production, in the Shi-Fuller (SF; Shi & Fuller, 1999) model it is also possible to have resonant production of sterile neutrinos in the presence of a lepton asymmetry resulting in an overabundance of leptons compared to antileptons. This adds an additional colder component of resonantly produced sterile neutrinos to the distribution (non-resonant production also still occurs), allowing for more freedom of allowed sterile neutrino masses.

The Neutrino Minimal Standard Model (νMSM; Asaka & Shaposhnikov, 2005) adds three sterile neutrinos to the standard model and would also explain the

baryon asymmetry of the universe. The heavier neutrinos have masses in the GeV range, while the lightest one has a keV mass, and is a good candidate for the dark matter. Boyarsky et al. (2009) explore the predictions of the νMSM in the presence of different degrees of lepton asymmetry L_6, to find the allowed parameter space for sterile neutrinos to avoid conflict with Andromeda x-ray bounds.

Independently of sterile neutrino modelling, it is also possible to consider more generic cases of multi-component dark matter (cold + warm). This becomes another two parameter problem where one can explore cold fraction and WDM temperature (analogous to L_6 and $m_{\rm sterile}$ parameters in the νMSM analysis).

The actual stringent values of the lower limits that these various analyses can place on WDM particle mass depend on the properties of the specific particle candidate being considered. Limits are often quoted for a generic thermal relic type particle, which has a simple exponential suppression of power at the cutoff. For a non-resonantly produced (NRP) sterile neutrino, the same constraints can be easily re-scaled from the thermal relic case, as the general form of the power spectrum maps nearly identically (Viel et al., 2005). However, as reviewed above, the presence of a resonant production mode for sterile neutrinos complicates the picture, as a colder component emerges. In the νMSM, the degree of lepton asymmetry determines the relative contributions of warmer and cooler contributions, so the lower mass limit will also depend on this second parameter.

The upper limit from x-ray non-detections described above is specific to sterile neutrino models of WDM, which are a focus here, although not the only option (for example, gravitino WDM).

As a convention throughout this paper, we will use $m_{\rm WDM}$ when referring to the generic thermal relic mass, and $m_{\rm sterile}$ when referring to sterile neutrino mass.

The rest of this analysis is organized as follows: in Chapter 2 we look first at the simplest (and likely ruled out) model of a thermal relic WDM particle, or equivalently a non-resonantly produced sterile neutrino. We introduce our

methodology in Section 2.1, including the computation of the fluctuation power spectrum, the construction of merger trees, and the adaptation of our semi-analytic model, GALFORM, to WDM. In Section 2.2 we predict satellite luminosity functions in galactic halos of different mass as a function of $m_{\rm WDM}$. In Section 2.3 we discuss the range of particle masses that are ruled out based upon various estimates of the Milky Way halo mass. A brief discussion of this limit in the context of other independent WDM constraints is presented, along with our conclusions, in Section 2.4. Then in Chapter 3, we also look at the more complex, and better motivated, RP sterile neutrinos of the νMSM model, to see what kind of limits we can place on this parameter space.

2

LIMITS ON $M_{\rm WDM}$

The number of subhalos predicted to survive in CDM and WDM galactic halos is a fundamental test for different candidates of potential DM candidates. In the case of CDM there are many more subhalos within galactic halos than there are observed satellites in the Milky Way, a discrepancy often - and incorrectly - dubbed "the satellite problem in CDM." In fact, it has been known for many years that inevitable feedback processes, particularly the early reionization of gas by the first stars and winds generated by supernovae, prevent visible galaxies from forming in the vast majority of the small subhalos that survive inside CDM halos (Bullock et al., 2000; Benson et al., 2002a; Somerville, 2002).

A "satellite problem," however, could exist in WDM because if $m_{\rm WDM}$ is too small, then there will be too few surviving substructures to account for the observed number of satellites. A limited version of this test was recently applied to surviving dark matter subhalos in high-resolution N-body simulations of WDM galactic halos by Polisensky & Ricotti (2011), who found a limit of $m_{\rm WDM} > 2.3$ keV, and by Lovell et al. (2014) who found a conservative lower limit of $m_{\rm WDM} > 1.1$ keV. In this paper we develop this theme further, however we apply the test *not* to dark matter subhalos but to visible satellites. This requires following the process of galaxy formation in galactic WDM halos, which allows a more direct comparison with observations of the Milky Way satellites and leads to stronger limits on $m_{\rm WDM}$. Since the number of surviving subhalos scales with the parent halo mass (Gao et al., 2004), these limits will depend on the mass of the Milky Way halo. Unfortunately, this mass is still very uncertain, with estimates rang-

ing from about 8×10^{11} to 2.5×10^{12} $M_\odot$ (e.g. Xue et al., 2008; Li & White, 2008; Guo et al., 2010; Deason et al., 2012; Rashkov et al., 2013; Piffl et al., 2013).

In this study we use the Durham semi-analytic model of galaxy formation, GALFORM, to follow galaxy formation in WDM models with different values of $m_{\rm WDM}$. Nierenberg et al. (2013) used a different semi-analytic model to study the redshift evolution of satellite luminosity functions for hosts of different masses, finding that compared to CDM, a $m_{\rm WDM} = 0.75$ keV particle captured better the observed evolution. Macciò & Fontanot (2010) also used a semi-analytic model, applied to N-body simulations of galactic halos of mass 1.22×10^{12} $M_\odot$ to set a lower limit of $m_{\rm WDM} > 1$ keV. This limit, however, is only valid for halos of this particular mass. Here, we use a version of GALFORM in which galaxy merger trees are computed using Monte Carlo techniques (calibrated on WDM N-body simulations). In this way, we are able to explore models with a wide range of halo masses and thus set limits on $m_{\rm WDM}$ for different values of the, as yet poorly known, Milky Way halo mass. Another important advantage of our method is that it does not suffer from the problem of spurious halo fragmentation complicating the interpretation of high resolution N-body WDM simulations.

Not surprisingly, only a very minor adjustment to the galaxy formation model in CDM is required in WDM to obtain a good match to a variety of observed properties of the local galaxy population, such as galaxy luminosity functions in various passbands. We then apply this model to derive the expected luminosity function of satellites of galaxies like the Milky Way and thus set strong constraints on the value of $m_{\rm WDM}$ as a function of the Milky Way halo mass.

2.1 Methods

2.1.1 The Warm Dark Matter Linear Power Spectrum

In the case where the warm dark matter consists of thermal relics, the suppression of small-scale power in the linear power spectrum, $P_{\rm WDM}$, can be con-

veniently parametrized by reference to the CDM power spectrum, $P_{\rm CDM}$. The WDM transfer function is then given by,

$$T(k) = \Big[\frac{P_{\rm WDM}}{P_{\rm CDM}}\Big]^{1/2} = [1 + (\alpha k)^{2\nu}]^{-5/\nu} \tag{2.1.1}$$

(Bode et al., 2001). Here, k is the wavenumber and following Viel et al. (2005) we take the constant $\nu = 1.12$; the parameter α can be related to the mass of the particle, $m_{\rm WDM}$ by

$$\alpha = 0.049\Big(\frac{\Omega_{\rm WDM}}{0.25}\Big)^{0.11}\Big(\frac{h}{0.7}\Big)^{1.22}\Big(\frac{\rm keV}{m_{\rm WDM}}\Big)^{1.11} h^{-1}{\rm Mpc} \tag{2.1.2}$$

(Viel et al., 2005), in terms of the matter density parameter, $\Omega_{\rm WDM}$, and Hubble parameter, $h = {\rm H}_0$ / (100 km s^{-1} Mpc^{-1}).

In the case where the WDM particle is a non-resonantly produced sterile neutrino, its mass $m_{\rm sterile}$, can be related to the mass of the equivalent thermal relic, $m_{\rm WDM}$, by requiring that the shape of the transfer function, $T(k)$, be similar in the two cases. Viel et al. (2005) give

$$m_{\rm sterile} = 4.43\Big(\frac{m_{\rm WDM}}{\rm keV}\Big)^{4/3}\Big(\frac{0.25(0.7)^2}{\Omega_{\rm WDM}h^2}\Big)^{1/3}{\rm keV}. \tag{2.1.3}$$

This conversion depends on the specific particle production mechanism (for a review see Kusenko, 2009); in the rest of this paper we will refer only to the thermal relic mass, $m_{\rm WDM}$, unless stated otherwise. We consider particles with masses, $m_{\rm WDM}$, ranging from 0.5 keV to 20 keV. Fig. 2.1 shows the linear power spectra for six of the 11 WDM models we have investigated, as well as for CDM.

We adopt values for the cosmological parameters that are consistent with the WMAP7 results (Komatsu et al., 2011): $\Omega_{\rm m} = 0.272$, $\Omega_{\rm b} = 0.0455$, $\Omega_\Lambda = 0.728$, $h = 0.704$, $\sigma_8 = 0.81$, $n = 0.96$. Two hundred merger trees were generated for each main halo mass and for each WDM particle mass.

2.1.2 Galaxy Formation Models

We calculate the properties of the galaxy population in our WDM models using the Durham semi-analytic galaxy formation model, GALFORM (e.g. Cole et al.,

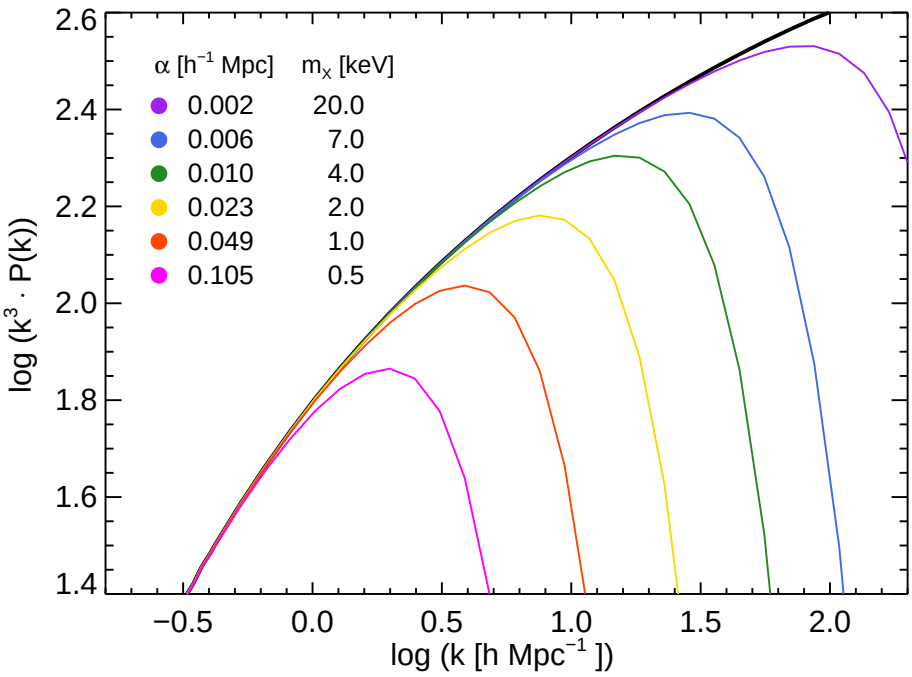

Figure 2.1: Linear power spectra (in arbitrary units) for warm and cold dark matter models. The thick black line shows CDM and the coloured lines various WDM models, labelled by their thermal relic mass and corresponding value of the damping scale, α, in the legend.

2000; Benson et al., 2003; Bower et al., 2006). Rather than applying it to merger trees obtained from an N-body simulation, we instead construct Monte Carlo merger trees using the Extended Press-Schechter (EPS) formalism (Press & Schechter, 1974; Bond et al., 1991; Bower, 1991; Lacey & Cole, 1993; Parkinson et al., 2008) to generate conditional mass functions for halos of a given mass. The standard formulation of the EPS formalism (in which the density field is filtered with a top hat in real space) is not applicable in the presence of a cutoff in the power spectrum. Instead, using a sharp filter in k-space produces a halo mass function in good agreement with the results of N-body simulations. We adopt this prescription which is justified and described in detail in Benson et al. (2013). A similar procedure was adopted by Schneider et al. (2013) but other authors, such as Smith & Markovic (2011) and Menci et al. (2012), have used a top hat filter in real space and then multiplied the resulting mass function by an *ad hoc* suppression factor. We do not apply the correction for finite phase-space density derived by Benson et al. (2013) because the effect of thermal velocities is negligible in the models we consider (Macciò et al., 2012; Shao et al., 2013). Halo concentrations were set according to the NFW prescription (Navarro et al., 1996, 1997), as described in Cole et al. (2000), thus explicitly taking into account the later formation epoch of WDM halos compared to CDM halos of the same mass. These concentrations are broadly in agreement with the WDM simulations of Schneider et al. (2012).

We use the latest version of GALFORM (Lacey et al. 2015, in prep.) which includes several improvements to the model described by Bower et al. (2006). The standard GALFORM model is tuned to fit a set of observed properties of the local galaxy population assuming CDM. Thus, an adjustment is required in the WDM case. On scales larger than dwarf galaxies at $z = 0$ there is little difference between WDM and CDM models. On smaller scales, the most important processes that influence galaxy formation are the feedback effects produced by the early reionization of the intergalactic medium and supernova feedback.

In GALFORM, reionization is modelled by assuming that no gas is able to cool in galaxies of circular velocity less than $v_{\rm cut}$ at redshifts less than $z_{\rm cut}$. For

CDM, the values $v_{\rm cut} = 30$ km s^{-1} and $z_{\rm cut} = 10$ result in a good approximation to more advanced treatments of reionization (Okamoto et al., 2008; Font et al., 2011). Supernovae feedback, on the other hand, is controlled by the parameter β, the ratio of the rate at which gas is ejected from the galaxy to the star formation rate. This ratio is assumed to depend on the circular velocity of the disc, $v_{\rm circ}$, as:

$$\beta = \left(\frac{v_{\rm circ}}{v_{\rm hot}}\right)^{-\alpha_{\rm hot}}, \tag{2.1.4}$$

where $v_{\rm hot}$ and $\alpha_{\rm hot}$ are adjustable parameters fixed primarily by the requirement that the model should match the local b_J- and K-band galaxy luminosity functions. In the Lacey et al. model, these parameters take on the values $v_{\rm hot} = 300$ km s^{-1} and $\alpha_{\rm hot}$ = 3.2. Since $v_{\rm circ}$ depends on the concentration of the host halo, which is lower for a WDM halo than for a CDM halo of the same mass (Lovell et al., 2012), we expect that a small adjustment to the parameters in eqn. 2.1.4 will be required to preserve the good match to the local luminosity functions.

Fig. 2.2 shows the b_J-band field galaxy luminosity function for different values of $\alpha_{\rm hot}$ for the case of a 2 keV particle. Here, $v_{\rm cut}$ and $z_{\rm cut}$ are set to the CDM values. (The reionization model mostly affects galaxies fainter than those included in estimates of the field luminosity function). The figure shows that only a small change in the value of $\alpha_{\rm hot}$ is required to achieve as good a fit to the measured b_J-band luminosity function as in the CDM case. The best fit for $m_{\rm WDM} = 3$ keV is obtained for $\alpha_{\rm hot} \sim 3.0$ (green line; assuming the same value of $v_{\rm hot} = 300$ km s^{-1} as in CDM). In general, we find that the local galaxy luminosity function in WDM models is well reproduced for a wide range of values of $m_{\rm WDM}$ by setting,

$$\alpha_{\rm hot}(m_{\rm WDM}) = 3.2 - 0.3\left(\frac{m_{\rm WDM}}{\rm keV}\right)^{-1} \tag{2.1.5}$$

(keeping the same values of $v_{\rm hot}$ and of $v_{\rm cut}$ and $z_{\rm cut}$ as above). This adjustment also results in acceptable matches to the K-band luminosity function, Tully-Fisher relation, size distribution and other observables. However, we find that

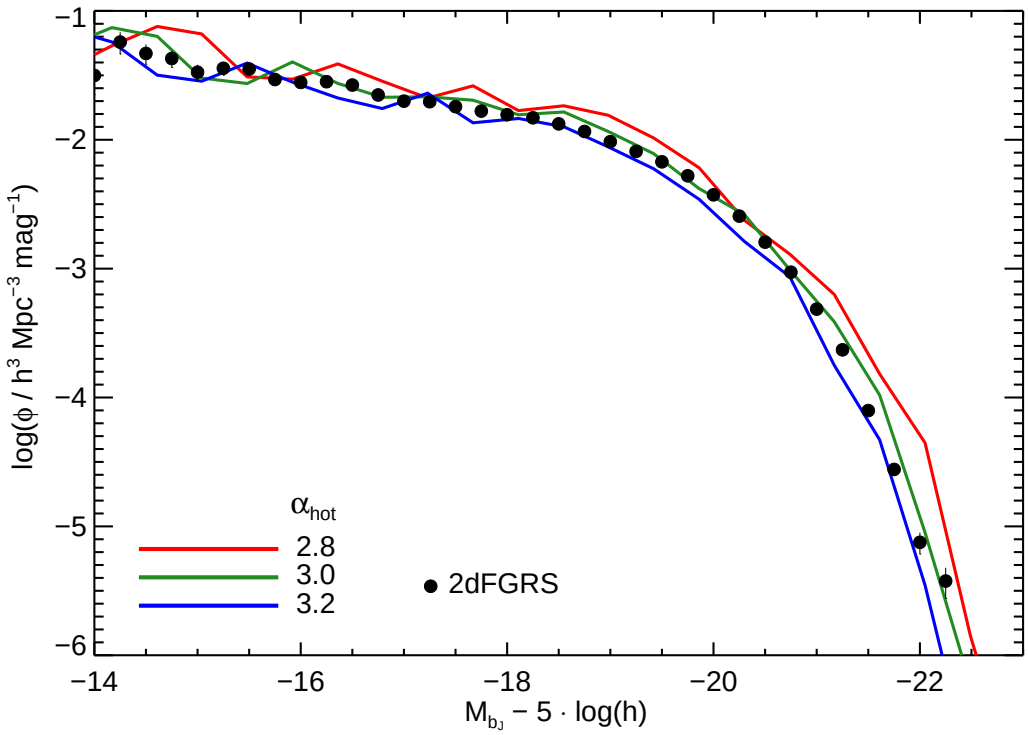

Figure 2.2: The b_J-band local galaxy luminosity function for $m_{\rm WDM}$ = 3 keV compared to the 2dFGRS determination (Norberg et al., 2002; indicated by circles). Coloured curves show the effect of varying $\alpha_{\rm hot}$, as shown in the legend

for $m_{\rm WDM} < 1.5$ keV, we cannot obtain acceptable models using eqn. 2.1.5. Kang et al. (2013) also found that it was not possible to find a consistent model of galaxy formation for such low mass WDM particles. Since these masses are, in any case, ruled out by observations of the Lyman-α forest, we restrict the rest of this analysis to the 9 models with particle masses larger than 1.5 keV.

In Section 2.3.2 we vary the adjustable parameters in our models of reionization and supernovae feedback to assess how they affect our inferred lower limits on the WDM particle mass. Throughout the remainder of this thesis, we will refer to the model described here as the 'fiducial' model.

2.2 Satellite Luminosity Functions

We now consider satellite systems, firstly those predicted by GALFORM to exist in halos of mass similar to that of the Milky Way's, and then the Milky Way's own system. We then describe the method we have adopted to compare the two.

2.2.1 The Predicted Satellite Population

We use the models described in Section 2.1.1 with final halo masses ranging from 5×10^{10} $M_\odot$ to 1×10^{13} $M_\odot$, a significantly wider range than that covered by recent estimates of the Milky Way's halo mass. The mass resolution of the merger trees is set to 1×10^6 $M_\odot$, which is below the free-streaming scale of our WDM models.

Fig. 2.3 shows the predicted cumulative V-band satellite luminosity functions for several examples. The three panels show results for $m_{\rm WDM}$ = 2, 3 and 20 keV and, within each panel, the effect of increasing the host halo mass from 8×10^{11} $M_\odot$ to 2.5×10^{12} $M_\odot$ is demonstrated. Increasing the host halo mass increases the number of satellites at all luminosities, and increasing the WDM particle mass increases the number of satellites particularly at fainter magnitudes. The number of bright satellites ($M_V \lesssim -12$) is insensitive to $m_{\rm WDM}$ because these satellites form in halos with mass above the cutoff scale in the WDM power spectrum.

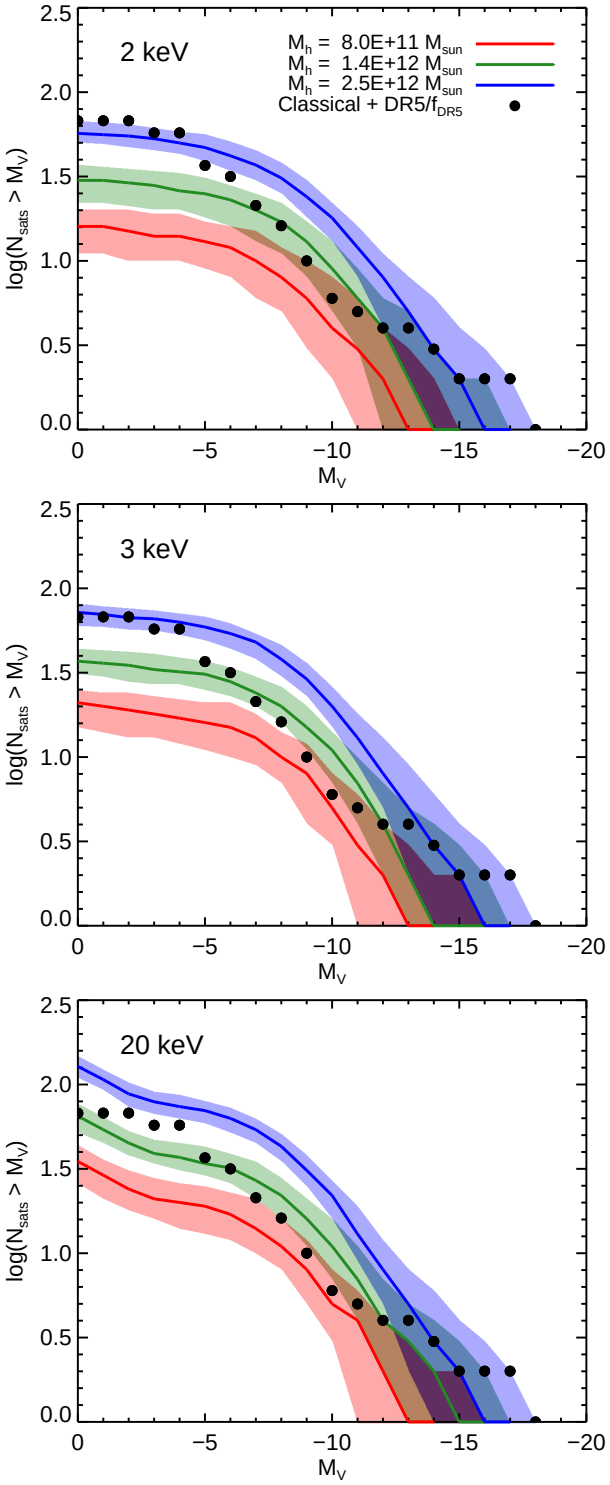

Figure 2.3: Satellite galaxy luminosity functions predicted by our fiducial semi-analytic model in galactic halos of different mass, for WDM particle masses, $m_{\rm WDM}$, of 2 keV, 3 keV and 20 keV, as indicated in the legend. The different coloured curves correspond to different host halo mass. The solid line in each case is the median cumulative V-band satellite luminosity function and the edges of each band indicate the 10th and 90th percentiles. For reference, the luminosity function of the 11 observed classical satellites, plus the DR5 satellites (scaled for sky coverage assuming an isotropic distribution) is indicated by the black dots.

2.2.2 The Observed Satellite Population

To determine whether a model produces a satisfactory number of satellites we make use of observations of the satellites around the Milky Way. While there have been recent censuses of satellites around galaxies outside the Local Group (e.g. Guo et al., 2011; Lares et al., 2011; Liu et al., 2011; Wang & White, 2012; Strigari & Wechsler, 2012) these tend to be limited to the brightest few. Many faint satellites have been observed around M31 (e.g. Martin et al., 2006, 2009, 2013; Ibata et al., 2007; McConnachie et al., 2009), but in this analysis we limit ourselves to studies of the population in our own galaxy.

There are eleven bright satellite galaxies around the Milky Way which were discovered in the previous century; these are dubbed the "classical satellites". In more recent years, the Sloan Digital Sky Survey (e.g. Adelman-McCarthy et al., 2007) has revealed a number of fainter satellite galaxies. For this analysis we focus on 11 additional satellites found in the SDSS Data Release 5 (DR5) (see summary in Tollerud et al., 2008), not double counting any classical satellites. This survey covers a fraction $f = 0.194$ of the sky, which is roughly 8000 square degrees, to a depth of around 22.2 in the g- and r- bands. We refer to these satellites here as the "DR5 satellites".

It is likely that there are yet more satellites in the DR5 region which have not been detected due to their faintness; at 260 kpc the survey is only complete to $M_V \approx -6$ (Koposov et al., 2008). Attempts to correct for the detection limits of the survey by assuming a given radial profile of the satellites predict a total satellite population of hundreds (e.g. Koposov et al., 2008; Tollerud et al., 2008).

2.2.3 Assessing Model Population Likelihoods

For the purposes of comparing our model predictions with satellite galaxy data, we will consider only those satellites brighter than M_V = -2, which is fainter than the magnitude of all the DR5 satellites. Since GALFORM only makes predictions for satellites which lie within the virial radius of the host halo, we limit our analysis of the real Milky Way satellites to those with a galactocentric distance less

than the virial radius of a particular halo in the semi-analytic calculation. Here, the virial radius is defined as the boundary of the region enclosing an overdensity, Δ, with respect to the critical density, where, for the spherical collapse model, $\Delta \approx 93$ (Eke et al., 1996).

In order to estimate the total number of satellites brighter than $M_V = -2$ that we would expect around the Milky Way, it is necessary to make some assumptions about the underlying distribution since it is not fully sampled. Firstly, we make the assumption that all the 'classical' satellites (those with apparent magnitudes brighter than $M_V \approx -8.5$) have been observed. This is probable, although our results would not change significantly even if one or two remained undetected behind the Milky Way disk.

Next, we assume that the underlying distribution of satellites is isotropic, so that the DR5 represents a geometrically unbiased sampling. This may be unrealistic because the eleven classical satellites of the Milky Way are known to lie in a 'pancake' structure oriented approximately perpendicular to the plane of the Milky Way disk (Lynden-Bell, 1976, 1982; Majewski, 1994; Libeskind et al., 2005). A large region of the DR5 footprint intersects this plane; if as yet undetected satellites also tend to lie in this disk, then the DR5 would provide a biased sampling of the true satellite population, leading us to overpredict the number of satellites that are necessary to match the data. This would have the effect of weakening our lower limit on $m_{\rm WDM}$. However, cosmological N-body simulations show that the preferentially flattened satellite distributions are restricted to the brightest satellites, and that as fainter and fainter populations are considered, their distribution tends to become increasingly isotropic (Wang et al., 2013).

Finally, we make the extremely conservative assumption that every satellite in the DR5 footprint area has been detected, so that no more faint satellites are lurking below the detection threshold. Given the survey's radial completeness limits, this is unrealistic. This assumption works in the sense of making our inferred lower limits on $m_{\rm WDM}$ conservative. If future or current surveys, such as Pan-STARRS, were to reveal even more faint satellites, our lower mass limits

would become correspondingly stronger.

To quantify whether the model satellite population is compatible with the MW data, we require that the model should produce at least as many satellites with $M_V < -2$ as are known to exist in the Milky Way. To find the likelihood of each model given the data, we calculate the probability that the predicted satellite population includes at least as many members falling within a region the size of the DR5 footprint, i.e. covering a fraction of the sky, $f = 0.194$, as the DR5 survey itself, which contains $n_{\rm DR5}$ satellites[1].

First, we define the number of classical Milky Way satellites (again within the virial radius of the model halo) to be $n_{\rm class}$. This number is subtracted from the total number of predicted satellites, $n_{\rm galform}$, to prevent double-counting in the DR5 region,

$$n_{\rm pred} = n_{\rm galform} - n_{\rm class} \tag{2.2.6}$$

Then, for this remaining population of $n_{\rm pred}$ satellites, we must find the likelihood that they are distributed such that at least as many satellites as are observed in DR5 fall in a region covering a fraction f of the total sky area. We find the probability, P, that a number between $n_{\rm DR5}$ and $n_{\rm pred}$ satellites lie in this region by assuming that a given satellite is equally likely to be found anywhere on the sky. Hence, P can be calculated from a binomial distribution,

$$P = \sum_{k=n_{\rm DR5}}^{k=n_{\rm pred}} \left(\frac{n_{\rm pred}!}{k!(n_{\rm pred}-k)!} \right) \cdot f^k \cdot (1-f)^{n_{\rm pred}-k} \tag{2.2.7}$$

Eqn. 2.2.7 gives the probability that any given realization of a halo merger tree, for a particular value of $m_{\rm WDM}$, within a given host halo mass, M_h, has produced enough satellites to be compatible with the Milky Way data. Since we have generated 200 merger trees for each WDM model at a given host halo mass, we take the average of the probabilities, P, computed for each individual host halo using eqn. 2.2.7.

[1]The value of $n_{\rm DR5}$ used will depend upon the virial radius of the halo we compare to.

If $\langle P \rangle$ is smaller than 0.05, we conclude that this model predicts too little substructure to account for the observations. Conversely, for each WDM particle mass, $m_{\rm WDM}$, we find the minimum host halo mass, M_h, for which $\langle P \rangle$ is larger than 5%. This value of $m_{\rm WDM}$ is therefore the limiting mass that cannot be excluded at 95% confidence.

2.3 Results: Limits on the WDM Particle Mass

In this section we present the constraints on the warm dark particle mass that follow from comparing our predictions for the satellite luminosity functions with the Milky Way data. We also discuss how our limits can be affected by uncertainties in our modelling of galaxy formation.

2.3.1 Fiducial Model

The constraints on the WDM particle mass as a function of host halo mass set by the method described in Section 2.2.3 are shown in the exclusion diagram of Fig. 2.4(a). Each point in the plot gives the smallest Galactic halo mass that has at least a 5% chance of hosting enough satellites to account for the observed number. Conversely, for a given Galactic halo mass, the minimum allowed WDM particle mass can be read off the x-axis. The shaded region shows the parameter space that is excluded. For example, if the Milky Way were found to have a mass of 1.5×10^{12} $M_\odot$, then the thermal relic dark matter particle must be more massive than 3 keV. The envelope of the exclusion region asymptotes to a value of 1.1×10^{12} $M_\odot$. Thus, for Milky Way halo masses below this value, all WDM particle masses are ruled out at 95% confidence by our model.

As an additional test we have applied the SDSS visibility limits to our satellite populations, in order to discern which could actually be detected by the survey. Using Eqn. 2 given in Tollerud et al. (2008), we find the threshold radius beyond which each of our satellites of a certain V-band magnitude would not be detected. Since the Monte Carlo based approach used here does not yield spatial information about the satellites, we use the radial distribution from

Anderhalden et al. (2013) (Fig. 4; very similar for CDM and WDM) in order to determine the probability that each satellite is inside this completeness radius. Then, generating a random value between 0 and 1, we reject the satellite from our culled sample if this value is larger than the calculated probability. This yields the population of satellites which would be observable by SDSS. The result of this exercise is shown in Fig. 2.4(a) by the dotted magenta line. The limits become more stringent since this selection eliminates most of the faintest satellites from the sample.

An accurate measurement of the Milky Way's halo mass, $M_{\rm h}$, could, in principle, rule out all astrophysically interesting thermally-produced WDM particles. Unfortunately, this measurement is difficult and subject to systematic uncertainties. Several methods have been used to estimate $M_{\rm h}$. (The values quoted below refer to different definitions of virial mass assuming different values of the limiting density contrast, Δ, as indicated by the subscript, M_Δ). A traditional one is the timing argument of Kahn & Woltjer (1959) which employs the dynamics of the Local Group to estimate its mass. Calibrating this method with CDM N-body simulations, Li & White (2008) find $M_{200} \sim 2.43 \times 10^{12}$ M$_\odot$, with a lower limit of $M_{200} = 8.0 \times 10^{11}$ M$_\odot$ at 95% confidence. A rather different method is based on matching the abundance of galaxies ranked by stellar mass to the abundance of dark matter halos ranked by mass in a large CDM N-body simulation. This technique gives upper and lower 10% confidence limits of $8 \times 10^{11} < M_{200} < 4.7 \times 10^{12}$ M$_\odot$ (Guo et al., 2010).

A third class of methods relies on the kinematics of tracer stars in the stellar halo to constrain the potential out to large distances. Using positions and line-of-sight velocities for 240 halo stars, Battaglia et al. (2005) find $6 \times 10^{11} < M_{100} < 3 \times 10^{12}$ M$_\odot$, depending on assumptions about the halo profile; using 2000 BHB stars out to 60 kpc, interpreted with the aid of simulations, Xue et al. (2008) find $8 \times 10^{11} < M_{102} < 1.3 \times 10^{12}$ M$_\odot$. Using a variety of tracers, Deason et al. (2012) find the mass within 150 kpc to be between 5×10^{11} M$_\odot$ and 1×10^{12} M$_\odot$. Most recently, Piffl et al. (2013) used a large sample of stars from the RAVE survey in conjunction with cosmological simulations to find $1.3 \times 10^{12} < M_{200} <$

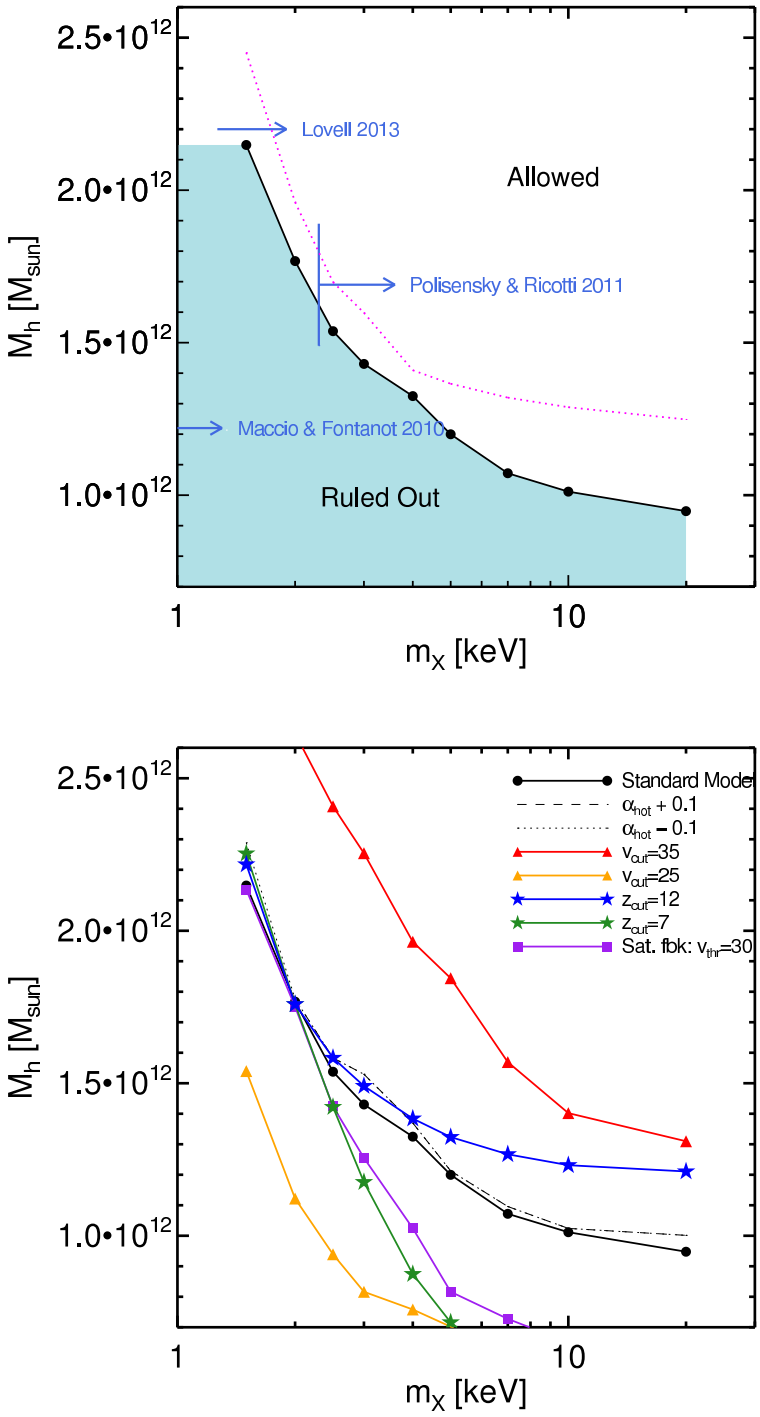

Figure 2.4: Top: exclusion diagram for thermal WDM particle masses, $m_{\rm WDM}$, as a function of the Milky Way dark matter halo mass, M_h; the shaded region is excluded. The lower limits reported by other authors, as well as the host halo masses they considered, are indicated by the arrows. The dotted magenta line shows the limit if satellites not visible to an SDSS-type survey are excluded. Bottom: sensitivity of our constraints to variations in the parameters of our galaxy formation model; the lines show the envelope of the exclusion region.

1.8×10^{12} $M_{\odot}$.

2.3.2 Sensitivity to Galaxy Formation Model Parameters

Given an assumption about the nature of the dark matter, the abundance of galactic satellites depends primarily on two key astrophysical processes: the reionization of hydrogen after recombination and feedback from supernovae explosions. The epoch during which the universe became reionized is constrained by temperature anisotropies in the microwave background and their polarization to lie in the range $8 \lesssim z_{\rm re} \lesssim 14$ (Planck Collaboration et al., 2013). Photoheating raises the entropy of the gas and suppresses cooling into halos of low virial temperature.

In GALFORM reionization is modelled by assuming that no gas cools in halos of circular velocity smaller than $v_{\rm cut}$ at redshifts lower than $z_{\rm cut}$. This simple prescription has been shown to be a good approximation to a more detailed semi-analytic model of reionization (Benson et al., 2002b) and to full gasdynamic simulations (Okamoto et al., 2008). In our fiducial model, the parameters take the values $v_{\rm cut} = 30$ km s^{-1} and $z_{\rm cut} = 10$. The simulations of Okamoto et al. (2008) suggest that $v_{\rm cut}$ is around 25 km s^{-1}, but Font et al. (2011) conclude that a value of $v_{\rm cut} = 34$ km s^{-1} is required to match the results of the detailed semi-analytical calculation of the effects of reionization given by Benson et al. (2002a). We explore the effect of varying both $v_{\rm cut}$ and $z_{\rm cut}$ within these bounds.

Supernova feedback is still poorly understood. In GALFORM, this process is modelled in terms of a simple parametrized power-law of the disc circular velocity with exponent $\alpha_{\rm hot}$ (eqn. 2.1.4). As discussed in Section 2.1.2, the parameter $\alpha_{\rm hot}$ is constrained – as a function of $m_{\rm WDM}$– by the strict requirement that the model should provide an acceptable fit to the observed local b_J-band galaxy luminosity function. This is a strong constraint which limits any possible variation of $\alpha_{\rm hot}$ to less than ± 0.1. Our simple parametrization ignores, for example, environmental effects (Lagos et al., 2013) but these are unlikely to make a significant difference to our conclusions so we do not consider them further. However we do consider a model in which the effects of feedback saturate below

$v_{\rm circ}$ = 30 km s^{-1}, similar to what Font et al. (2011) argue is required to explain the variation of metallicity with luminosity observed in the population of Milky Way satellites.

The effects of varying the galaxy formation model parameters (retaining agreement with the local field galaxy luminosity function) on our constraints on $m_{\rm WDM}$ as a function of $M_{\rm h}$ are shown in Fig. 2.4(b). Varying $\alpha_{\rm hot}$ has a very small effect; varying $z_{\rm cut}$ affects, to some extent, the limits for WDM particle masses greater than 2-3 keV. The main sensitivity is to the parameter $v_{\rm cut}$ which has a strong effect on the number of small halos which are able to form stars. At fixed halo mass, lower values of $v_{\rm cut}$ weaken the limits on $m_{\rm WDM}$ whereas larger values strengthen them. The range considered here, $25 < v_{\rm cut}/{\rm km\ s^{-1}} < 35$, is realistic according to current understanding of the process of reionization.

2.4 Discussion and Conclusions

The cutoff in the linear power spectrum of density fluctuations produced by the free streaming of warm dark matter particles in the early universe provides, in principle, the means to search for evidence of these particles. If the particle mass is in the keV range, the cutoff occurs on the scale of dwarf galaxies and no primordial fluctuations are present on smaller scales. Thus, establishing how smooth the universe is on these scales could reveal the existence of WDM or, since the cutoff length scales inversely with the particle mass, set limits on its mass. The traditional method for testing the smoothness of the density field at early times is to measure the flux power spectrum of the Lyman-α forest in the spectra of high redshift quasars. The most recent lower limit on the WDM particle mass using this method on data at redshifts $z \sim 2-6$ is that set by Viel et al. (2013), $m_{\rm WDM} \geq 3.3$ keV (2σ), for thermally produced warm dark matter particles.

A different way to estimate the clumpiness of the matter density field on small scales, this time at the present day, is to count the number of substructures embedded in galactic halos. The most direct way to do this is to count the satel-

lites that survive in such halos but these are so faint that sufficient numbers can only be found in our own Milky Way galaxy and M31. Counting the Milky Way satellites thus provides a test of WDM which is independent from and complementary to the Lyman-α forest constraint. There are several complications that need to be taken into account when carrying out this test. Firstly, a suitable property to characterize the satellite population needs to be identified. The maximum of the circular velocity curve, $v_{\rm max}$, is often used for this purpose, but this quantity is not directly measurable for the Milky Way's satellites. The luminosities of satellites, on the other hand, are accurately measured, but using this as a test of WDM requires the ability to predict the satellite luminosities and this, in turn, requires modelling galaxy formation. This is the approach we have adopted in this paper where we have made use of the semi-analytic model, GALFORM. This model has the virtue that it gives a good match to the field galaxy luminosity function in various bands and has been extensively tested against a variety of other observational data. The $v_{\rm max}$ test was carried out by Polisensky & Ricotti (2011) and by Lovell et al. (2014) but the uncertainty in the satellites' values of $v_{\rm max}$ introduces some uncertainty in the limits set.

The second complication is the requirement to understand the completeness of the satellite sample. The Milky Way has a population of 11 bright or "classical" satellites which is thought to be complete (although one or two bright satellites could be lurking behind the Galactic Plane, too small a number to affect our conclusions) and a population of faint and ultrafaint satellites that have been discovered in the fifth of the sky surveyed by the SDSS. While the classical satellites are known to be distributed on the thin plane, identified by Lynden-Bell (1976), it is not known if the SDSS sample is also anisotropic. Large N-body CDM simulations suggest that it is only the brightest satellites that lie on a plane whereas more abundant populations tend to be much less anisotropically distributed (Wang et al., 2013). Here we assume that the spatial distribution of the Milky Way satellites other than the classical ones is isotropic. If this assumption were incorrect, we would overestimate the number of satellites which would cause us to overestimate the minimum WDM particle mass required to

have enough satellites in a halo of a given mass. The simulations of Wang et al. (2013) suggest that this effect is unlikely to be large.

The third complication of our method is the difficulty in assessing possible systematic effects arising from uncertainties in our galaxy formation model. As we discussed in Section 2.3.2, the main source of uncertainty is our treatment of the inhibiting effect of the early reionization of the intergalactic medium on the cooling of gas in small halos. We model this process in a relatively simple way which, however, has been validated both by realistic semi-analytic calculations (Benson et al., 2002b) and by full cosmological hydrodynamic simulations (Okamoto et al., 2008). Another uncertainty arises from the fate of satellites prior to merging with the central galaxy: we do not currently consider tidal disruption effects in our model, meaning that all satellites survive until the point of merging. If tidal destruction is an important phenomenon, which may be especially true for WDM, then we would expect fewer surviving satellites in our models. This would have the net effect of increasing further our lower limits on $m_{\rm WDM}$.

Since the number of surviving subhalos is a strong function of the parent halo mass, our limits on $m_{\rm WDM}$ depend on the mass of the Milky Way halo which, unfortunately, is still uncertain to within a factor of at least a few. For our fiducial model of galaxy formation, we find that if the halo mass is less than 1.1×10^{12} $\mathrm{M}_\odot$, then *all* values of $m_{\rm WDM}$ are ruled out at 95% confidence for the case of thermally-produced WDM particles. If, however, the mass of the halo is greater than 1.3×10^{12} $\mathrm{M}_\odot$, then, at the same confidence level, all masses greater than $m_{\rm WDM} = 5$ keV are allowed and if it is greater than 2×10^{12} $\mathrm{M}_\odot$, then all masses greater than $m_{\rm WDM} = 2$ keV are allowed. If the main parameter in our model of reionization, $v_{\rm cut}$, had a value of 35 km s^{-1}, then most (thermal) masses of astrophysical interest would be ruled out even if the mass of the halo is 2×10^{12} $\mathrm{M}_\odot$, but if this parameter is only 25 km s^{-1}, then only masses below $m_{\rm WDM} = 2.5$ keV are ruled out for halo masses less than 1×10^{12} $\mathrm{M}_\odot$. By contrast, using the abundance of dark matter subhalos as a function of $v_{\rm max}$, Lovell et al. (2014) were only be able to set a lower limit of $m_{\rm WDM} = 1.3$ keV for dark matter halos of mass 1.8×10^{12} $\mathrm{M}_\odot$.

Our limits on the WDM particle mass from the abundance of satellites in the Milky Way are compatible with those set by the Lyman-α forest constraints, except, of course, that they depend on the mass of the Milky Way halo. The value of the most recent lower limit ($m_{\rm WDM} = 3.3$ keV) derived from the Lyman-α forest requires the halo mass to be $M_{\rm h} > 1.4 \times 10^{12}$ M$_\odot$ in order for there to be enough satellites in the Milky Way. All these limits apply only to thermally produced WDM and need not exclude specific warm candidates such as sterile neutrinos. In this case (and also for other types of WDM), there could also be additional resonantly produced particles that could behave as cold dark matter, resulting in a different small scale behaviour of the linear density power spectrum, depending on the mass and formation epoch of these particles.

Sterile neutrinos can decay and emit a narrow x-ray line. The absence of such a line in the x-ray spectra of galaxy clusters can be used to set an *upper* limit to $m_{\rm WDM}$ but this depends in the sterile neutrino production mechanism. For example, for non-resonant production, Abazajian et al. (2001) have set an *upper* limit of $m_{\rm sterile} \lesssim 5$ keV which would correspond to a thermal mass of ~ 1 keV.

The constraints presented in this study would become much tighter if the mass of the Milky Way halo could be measured accurately. While the recent RAVE results (Piffl et al., 2013) are encouraging, it is to be hoped that the forthcoming GAIA satellite mission will allow a better understanding of the systematic effects that complicate these kinds of measurements. In the meantime, gravitational lensing effects such as the flux ratio anomaly in multiply-lensed quasar images may provide a direct measurement of the amount of substructure present in galactic dark matter halos (Miranda & Macciò, 2007; Xu et al., 2013). This is a powerful method that could, in principle, provide a conclusive test of whether the dark matter is cold or warm.

3

νMSM RESONANTLY-PRODUCED STERILE NEUTRINOS: LIMITS

3.1 The νMSM

The sterile neutrino is an attractive dark matter candidate because it is independently well-motivated by particle physics, as well as having the right properties of a successful DM candidate. The νMSM (Asaka & Shaposhnikov, 2005) is an extension of the standard model which adds three sterile neutrinos in addition to the three active neutrinos, and could account for the observed baryon asymmetry and neutrino oscillations. In addition to two $\sim$GeV-mass sterile neutrinos, the third $\sim$keV-mass sterile neutrino is a DM candidate which falls in the broad range of "warm" models. This possibility motivates us to consider sterile neutrinos in this mass range as dark matter candidates to see what astrophysical constraints can be placed upon the proposed particles.

In Chapter 2, we determined the limits that MW satellite galaxy formation could establish for sterile neutrinos generated by non-resonant oscillations (which correspond directly to the thermal relic masses quoted more frequently throughout this work). But this model has essentially been ruled out (if sterile neutrinos alone are to comprise the dark matter) by not being able to simultaneously satisfy Lyman-α and M31 x-ray bounds.

However, in the presence of a lepton number asymmetry of the universe (which has not yet been well-constrained), resonant sterile neutrino production (RP) also proceeds, adding a kinematically colder population of sterile neutrinos

at a given mass. Unlike the DW sterile neutrinos in Chapter 2, these resonant sterile neutrinos of the same mass are no longer necessarily ruled out: at any given particle mass, this colder component lends more power to smaller scales than the simple pure-WDM case. Therefore the bounds from Lyman-α or satellite counting studies will be shifted down.

In the νMSM as presented in Boyarsky et al. (2009), the lepton asymmetry L_6 is a free parameter, defined as $L_6 = 10^6(n_{\nu_e} - n_{\bar{\nu}_e})/s$, where n_{ν_e}, $n_{\bar{\nu}_e}$ and s are the neutrino, antineutrino and entropy densities, respectively. According to Boyarsky et al. (2009), the maximum value of L_6 set by maximum CP violation is $L_6^{\max}$=700. In the case of no lepton asymmetry ($L_6 = 0$), the resonant production mechanism is shut off and we return to the (ruled out) DW non-resonant scenario of Chapter 2.

3.2 Methods

In this part of the analysis, we will examine sterile neutrino models with L_6 ranging from 0 to 700. Figure 3.1 shows the power spectra for sterile neutrinos of six different masses $m_{\rm sterile} = 1, 2, 3, 4, 10, 20$ (each panel) for several L_6 parameters (coloured lines). The location of the cutoff is not monotonic with L_6. As the degree of asymmetry increases, so does the fractional contribution of the (colder) resonantly-produced component. But the momentum distribution of the RP particles also depends upon L_6 such that the 'cold' component becomes warmer for high values of the asymmetry parameter. Note the maximum amount of small-scale power tends to peak around $L_6 \sim 25$ for the lower-mass sterile neutrinos, and around $L_6 \sim 2 - 8$ for the higher-mass particles.

We have repeated the same methodology described in Chapter 2 to use GALFORM to predict galaxy formation in halos generated from EPS merger trees. Here, in contrast to Chapter 2, we have *not* independently re-adjusted feedback parameter $\alpha_{\rm hot}$ for each case however. After running a few tests with small variations to $\alpha_{\rm hot}$, we did not find significant differences to our final results, and therefore used the parameterization of Eqn. 2.1.5 independently of different L_6

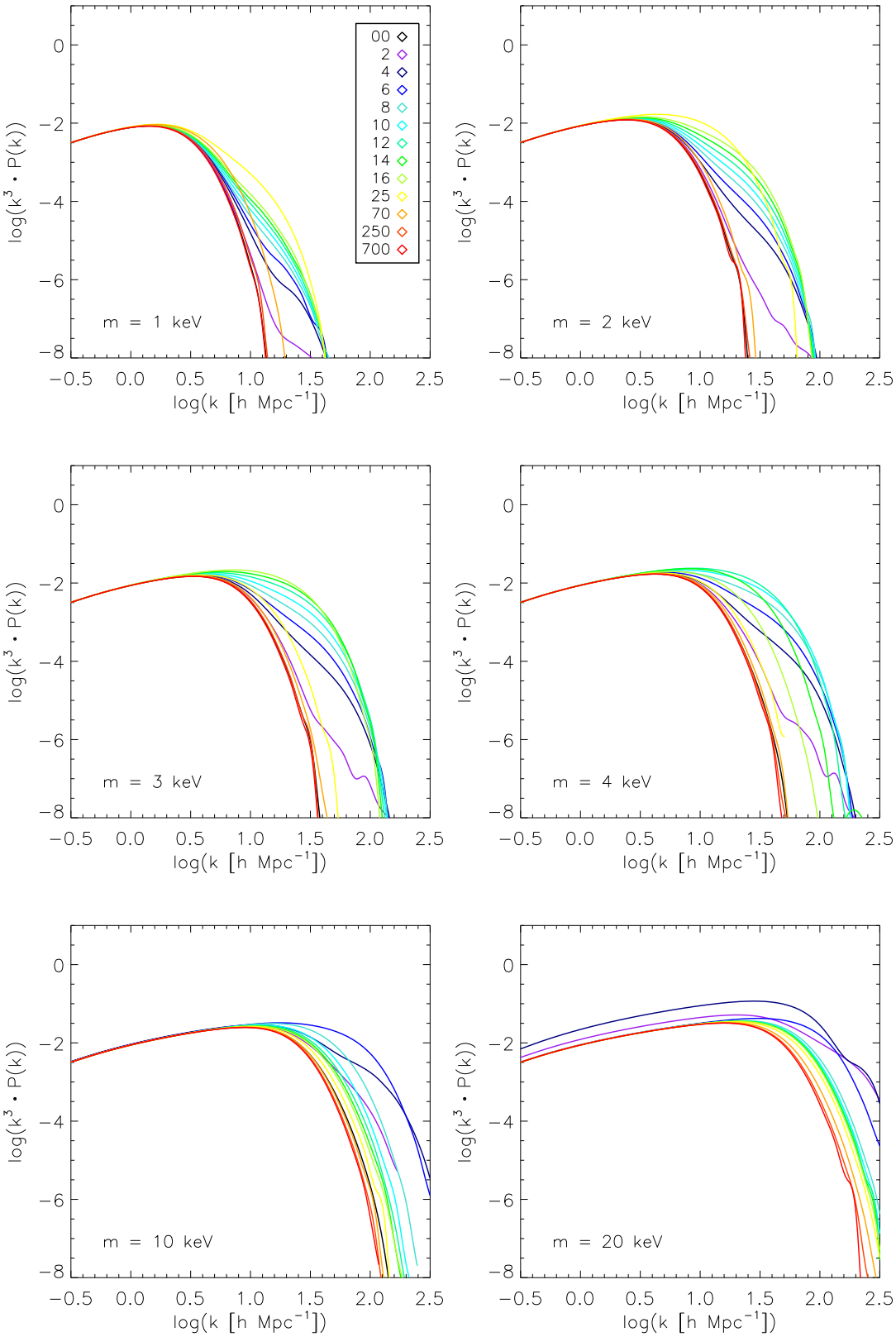

Figure 3.1: Sample linear power spectra for various particle mass and lepton asymmetry parameters. Each panel shows the effect of varying lepton asymmetry (coloured lines) for the sterile neutrino mass indicated in the lower left legend.

values.

3.3 Results

The results are shown in Figure 3.2. Here we show a similar particle-mass halo-mass relation to that which was presented earlier in Figure 2.4 for the simpler case. Note that this plot differs in that the particle masses are now for m_{sterile} (sterile neutrinos) instead of m_{WDM} in Figure 2.4, because with the introduction of RP, there is no direct thermal "equivalent" of a given m_{sterile}. Note also that the y-axis scale now encompasses a much wider range of halo masses, most of which are incompatibly heavy with respect to observations.

The lines on the plot show the minimum MW halo mass required, that would host enough satellites to be compatible with observations, for a given m_{sterile}. Each coloured line demonstrates this relationship for different asymmetry parameters L_6, as indicated in the legend. The zero-asymmetry case, in which there is no non-resonant contribution to the sterile neutrino population, is shown in black. For all cases of lepton asymmetry, we see the same general trend that for a less massive particle candidate to be allowed, the mass of the MW halo is required to be greater. Note that there are a few upturns in the lines plotted, showing exceptions to this trend. In these cases we are seeing the effect of the resonant production: the momentum distribution function shifts up faster with L_6 for higher-mass particles, so that in certain cases the lighter particle has a "cooler" distribution. If we assume the upper limit of this value allowed by recent measurements is $M_{\text{MW}} \leq 2.5 \times 10^{12}$ $\text{M}_\odot$ then the 1 keV case is completely ruled out, and the 2 keV case only permitted if $L_6 \sim 25$. If $M_{\text{MW}} \leq 1.0 \times 10^{12}$ $\text{M}_\odot$ then all particles $m_{\text{sterile}} \leq 10$ keV are ruled out, and a 20 keV sterile neutrino only permitted if $2 \lesssim L_6 \lesssim 14$.

There have been recent hints of the 7 keV sterile neutrino in the x-ray spectra of the MW, M31 and a sample of 73 bright clusters (Boyarsky et al., 2014a,b; Bulbul et al., 2014, respectively). The detection of a $\sim$ 3.5 keV emission line is not a definitive sign of a sterile neutrino decay (and could be attributed to other

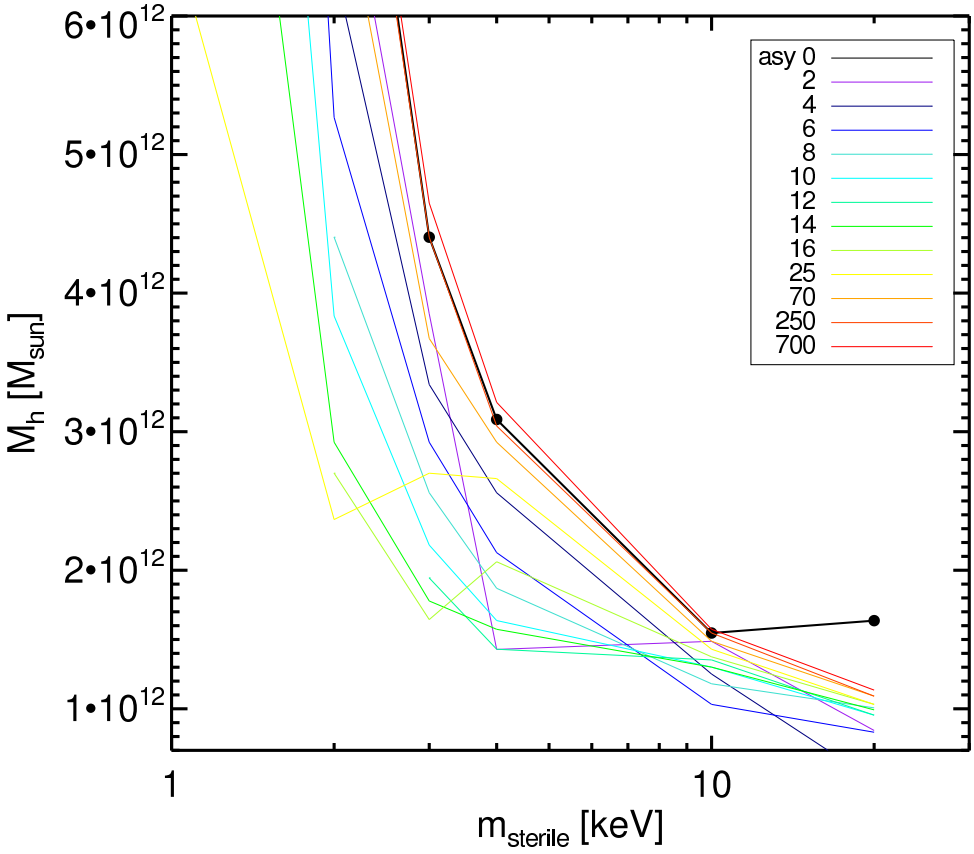

Figure 3.2: Exclusion diagram demonstrating the minimum value of the Milky Way halo mass required to be compatible with a given sterile neutrino mass, depending on the degree of lepton asymmetry (indicated by the coloured lines). All results shown here are for our fiducial model of galaxy formation.

galactic phenomena) but it does lead us to consider the 7 keV model with special focus. While we do not yet have the spectra for the 7 keV models in time for the publication of this work, we can extrapolate between the 4 keV and 10 keV data which we have analyzed. Referring again to Figure 3.2, we can see that at 7 keV, if there is no lepton asymmetry then $M_{\rm MW}$ would have to be larger than $\sim 2 \times 10^{12}$ $M_\odot$ to be compatible. For the most optimistic case, L_6 in the 2-16 range, then the mass could be as low as $\sim 1.4 \times 10^{12}$ $M_\odot$.

3.4 Discussion/Conclusions

In this Chapter, we have applied the satellite galaxy formation test to various sterile neutrino WDM models in order to place co-constraints on the values of the WDM particle mass $m_{\rm sterile}$, the lepton asymmetry parameter L_6 and the Milky Way halo mass. For a given halo mass, the constraint on particle mass is strong when there is no lepton asymmetry, and becomes more lenient as L_6 increases (along with the contribution of the colder RP sterile neutrinos). This trend reverses after some peak L_6 (which depends on particle mass) as the RP component becomes warmer until the $M_{\rm h}$-$m_{\rm sterile}$ constraint relation resembles the zero-asymmetry (100% NRP) scenario.

Compared to the analysis in Chapter 2, varying L_6 for sterile neutrino models allows more freedom for particles of a given mass to meet the success criteria defined here, and not be ruled out. Given recent measurements of the MW mass and taking an upper limit of $M_{\rm MW} \leq 2.5 \times 10^{12}$ $M_\odot$, $m_{\rm sterile}$ as low as 2 keV are permitted for the peak $L_6 = 25$. Again, further and more accurate estimates of $M_{\rm MW}$ will be useful in giving firmer lower limits on the particle mass.

As reviewed in Section 2.2.3, the satellite formation 'failure' threshold is very conservative in assuming that the SDSS DR5 survey leaves no faint dwarfs undetected. We anticipate that in the future as more ultrafaint satellites are discovered, the constraints from Figure 3.2 will shift to higher masses.

4

CONCLUSIONS AND FUTURE POSSIBILITIES

In this work we have examined satellite galaxy formation in WDM scenarios. We used the dwarf galaxies of the Milky Way as a benchmark to determine which WDM models were compatible with observations, and thus set lower limits on allowed particle masses.

To achieve this, we generated many Monte Carlo halo merger trees for each WDM model using the Extended Press Schechter formalism with a sharp k-space filter. These trees were processed with the GALFORM semi-analytic model of galaxy formation, and the strength of supernova feedback was decreased for decreasing particle mass to compensate for the correspondingly smaller concentrations for subhalos of an equivalent mass. From these re-tuned models, we were able to predict satellite luminosity functions for host halos spanning a range of mass consistent with recent measurements of the Milky Way, and use them to make a direct comparison to the luminous dwarfs detected in our own galaxy. Using 200 possible merger histories per particle mass, per halo mass sampled, we were able to determine at 95% confidence which WDM particle masses were ruled out for a given value of the halo mass. We conclude that for host halos less massive than 1×10^{12} $M_\odot$, all "astrophysically interesting" WDM models are ruled out. At a value of $M_{\rm MW} = 1.5 \times 10^{12}$ $M_\odot$, $m_{\rm WDM}$ is constrained to be larger than 2.5 keV. A relic mass as small as $m_{\rm WDM} = 1.5$ keV is allowed if the halo is more massive than 2×10^{12} $M_\odot$.

Next we considered that there is a level of uncertainty in our results stemming from a few free parameters in our semi-analytic model which are not

well-constrained. There is some flexibility in setting the parameters determining reionization and supernova feedback in the model, and these choices (particularly reionization) can affect disproportionately the smallest galaxies we are interested in. By making adjustments that did not appreciably change the field galaxy luminosity function, we explored how strongly these parameter variations affected the relationship between the lower mass limits. We found that the results were very sensitive to the threshold 'filtering mass' of reionization, below which cooling cannot occur after the universe is reionized. The redshift of reionization was also important at larger particle masses; we allowed for a range $z_{\rm rei} = 7 - 12$. Including the type of "saturated feedback" implemented in the Font et al. (2011) model - although we saturated at a lower threshold - also had an effect in expanding the allowed $m_{\rm WDM}$-$M_{\rm MW}$ parameter space.

After establishing limits for particles whose initial velocity distribution results in a linear power spectrum of fluctuations featuring a simple exponential suppression beyond some cutoff wavenumber (thermal relics and non-resonantly produced sterile neutrinos), we next considered more complex models. The Neutrino Minimal Standard Model (Asaka & Shaposhnikov, 2005) is physically well-motivated and would introduce a $\sim$keV mass sterile neutrino as a WDM candidate. In the presence of an existing lepton asymmetry, a population of cooler resonantly-produced sterile neutrinos will be generated in the Shi & Fuller (1999) mechanism. The amount of resonant production as well as the momentum distribution functions of the particles both depend on the degree of the asymmetry, leading to more nuanced features in the power spectra. We again used GALFORM with the EPS trees to study the satellite abundance of MW-like systems as a function of the three parameters of sterile neutrino mass, lepton asymmetry and host halo mass. The "cooling effect" or resonant production on the $m_{\rm sterile}$ limits was maximized for lepton asymmetries $L_6 \sim 12 - 25$. For example, if $M_{\rm MW} = 1.5 \times 10^{12}$, the minimum particle mass is $m_{\rm sterile} \geq 10$ / 3 /10 keV for L_6 = 0 / 16 / 70, respectively.

The constraints on WDM set here are consistent with the findings of other related studies of structure formation involving a suppression of small-scale

power. Some of the most robust limits have been imposed by the fluctuations in the Lyman-α forest from $z \approx 2-6$, which Viel et al. (2013) used recently to place a lower limit of $m_{\rm WDM} \geq 3.3$ keV. For us, this corresponds to a halo mass of $M_{\rm h} > 1.4 \times 10^{12}$ M$_\odot$ in our standard model. Analyses of reionization, GRBs, lensing flux anomalies and other phenomena have found limits of $m_{\rm WDM} \gtrsim 0.5-2$ keV. Previous studies of subhalo abundance making comparisons to the Milky Way have found similar mass limits. Here we have the power to strengthen such constraints, given an accurate measurement of the Milky Way mass, which may become more exact with upcoming surveys.

One application of the WDM galaxy formation models used here would be to apply the semi-analytic models to N-body simulations of WDM rather than Monte Carlo trees. This would enable a more detailed look at the galactic features predicted in WDM models, such as radial distribution of luminous satellites or the properties of the stellar halo. As the remnant of tidally stripped material from satellites accreting onto the main system, the stellar halo provides an informative record of the merger history of a galaxy. The Milky Way's own stellar halo includes roughly a billion stars and contains many substructures such as stellar streams, for example the prominent Sagittarius stream for which the donor Sagittarius Dwarf satellite is seen mid-disruption. Other nearby galaxies are also seen to have structure-rich stellar halos with identifiable stream and shell features. Using techniques like the Cooper et al. (2010) particle-tagging method, it is possible to make predictions for the formation of stellar halos in different cosmological models: a semi-analytic galaxy formation model is run on top of a high resolution numerical simulation, and the stars that form are linked to individual dark matter particles for the entirety of the simulation. In the original study, Cooper et al. (2010) performed this tagging for several MW-mass CDM halos, and found a great variety of morphologies and tidal features among the halos formed.

The stellar halo of a WDM galaxy might be anticipated to have some differences compared with a CDM halo, which could potentially be discerned through the kind of detailed observations that will be made with Gaia and other upcom-

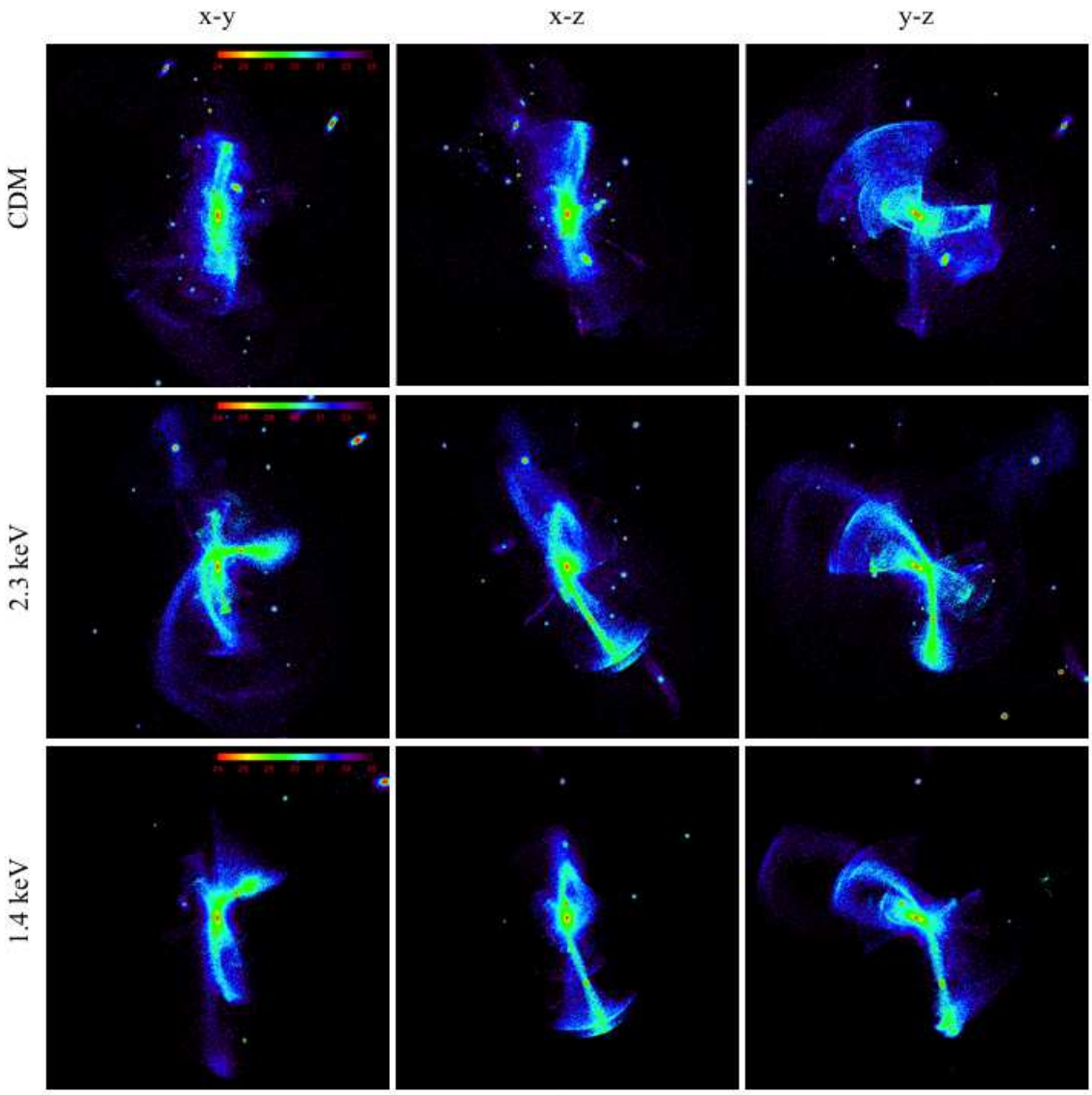

Figure 4.1: Surface brightness profiles for stellar halos in the case of CDM, $m_{\mathrm{WDM}} = 2.3$ keV and $m_{\mathrm{WDM}} = 1.4$ keV, shown from top to bottom, respectively. From left to right, the panels display three different projections of the same stellar halo in each case. All results here are for the Aquarius A halo.

ing surveys. The age, metallicity, spatial distribution and kinematics of halo stars are all potentially useful probes of the dark matter properties. Preliminary studies that we have done of WDM halos suggest that their overall morphology is smoother than for CDM, with less small-scale "clutter" and broader tidal streams. This makes sense as the same satellite progenitors will be less concentrated in WDM (although conversely there are fewer small subhalos present in WDM to dynamically heat the streams, but this appears to be a less important effect). As an example, Figure 4.1 illustrates the surface brightness profiles of the same stellar halo for three DM particles. Further analysis could be done here in quantifying the predictions of stellar halo structure, age and metal enrichment for different DM models in order to test directly against existing and future halo tracer star data.

Reionization studies are another topic to which WDM semi-analytics could be applied. As indicated in several previous studies of reionization in WDM universes (Barkana et al., 2001; Yoshida et al., 2003; Biermann & Kusenko, 2006; Schultz et al., 2014), it is considered a challenge for many models to form enough structure at early redshifts, and produce sufficient amounts of reionizing photons by redshift $z \approx 10$. Most of the previous studies have been based on N-body simulations alone, with some hydrodynamical simulations for specific relic masses. Here we would use the star formation information output by the galaxy formation model, and process large numbers of merger trees to get a good statistical measure of when reionization occurs for different WDM particles, and for different GALFORM model parameters. The framework for this was developed by Benson et al. (2002b,a), who modelled reionization within their semi-analytic model self-consistently for CDM. This would be particularly interesting for the case of resonantly produced sterile neutrinos, where there might be an earlier presence of star-forming structure than for other WDM models. Biermann & Kusenko (2006) find that the x-ray decays of sterile neutrinos can accelerate star formation and hasten reionization, which is also a potential feature that could be added to our semi-analytic model.

One caveat to this is the possibility of filamentary star formation preceding

halo star formation in WDM models (Gao & Theuns, 2007; Gao et al., 2014). This could affect reionization timelines for WDM models, and we do not currently have a framework for including filament-trees in our semi-analytic model.

In summary, WDM models encompass a range of particles which could be good candidates for the dark matter. However, these models are often found to be in tension with small-scale and high-redshift observations. We come to similar conclusions here, finding that "pure" WDM particles of interesting mass are difficult to reconcile with the satellite population of the Milky Way, although results do vary with halo mass. It seems that the future of WDM models is shifting towards "mixed" or "cool" dark matter, such as that generated by resonant production of sterile neutrinos, which we have also looked at. Until a confirmed detection of the DM particle is reported, such cosmological tests provide a useful way of evaluating different candidates. Our own results will be strengthened with the discovery of more satellites around our own galaxy (and M31), as well as firmer measurements of our galaxy's mass.

BIBLIOGRAPHY

Abazajian K., Fuller G. M., Tucker W. H., 2001, ApJ, 562, 593

Adelman-McCarthy J. K. et al., 2007, ApJS, 172, 634

Anderhalden D., Schneider A., Macciò A. V., Diemand J., Bertone G., 2013, Journal of Cosmology and Astroparticle Physics, 3, 14

Angulo R. E., Hahn O., Abel T., 2013, MNRAS, 434, 3337

Asaka T., Shaposhnikov M., 2005, Physics Letters B, 620, 17

Avila-Reese V., Colín P., Valenzuela O., D'Onghia E., Firmani C., 2001, ApJ, 559, 516

Barkana R., Haiman Z., Ostriker J. P., 2001, ApJ, 558, 482

Battaglia G. et al., 2005, MNRAS, 364, 433

Benson A. J., Bower R. G., Frenk C. S., Lacey C. G., Baugh C. M., Cole S., 2003, ApJ, 599, 38

Benson A. J. et al., 2013, MNRAS, 428, 1774

Benson A. J., Frenk C. S., Lacey C. G., Baugh C. M., Cole S., 2002a, MNRAS, 333, 177

Benson A. J., Lacey C. G., Baugh C. M., Cole S., Frenk C. S., 2002b, MNRAS, 333, 156

Biermann P. L., Kusenko A., 2006, Physical Review Letters, 96, 091301

Bode P., Ostriker J. P., Turok N., 2001, ApJ, 556, 93

Bond J. R., Cole S., Efstathiou G., Kaiser N., 1991, ApJ, 379, 440

Bower R. G., 1991, MNRAS, 248, 332

Bower R. G., Benson A. J., Malbon R., Helly J. C., Frenk C. S., Baugh C. M., Cole S., Lacey C. G., 2006, MNRAS, 370, 645

Boyarsky A., Franse J., Iakubovskyi D., Ruchayskiy O., 2014a, ArXiv e-prints

Boyarsky A., Ruchayskiy O., Iakubovskyi D., Franse J., 2014b, ArXiv e-prints

Boyarsky A., Ruchayskiy O., Shaposhnikov M., 2009, Annual Review of Nuclear and Particle Science, 59, 191

Boylan-Kolchin M., Bullock J. S., Kaplinghat M., 2011, MNRAS, 415, L40

Bulbul E., Markevitch M., Foster A., Smith R. K., Loewenstein M., Randall S. W., 2014, ApJ, 789, 13

Bullock J. S., Kravtsov A. V., Weinberg D. H., 2000, ApJ, 539, 517

Cole S., Lacey C. G., Baugh C. M., Frenk C. S., 2000, MNRAS, 319, 168

Colín P., Avila-Reese V., Valenzuela O., 2000, ApJ, 542, 622

Cooper A. P. et al., 2010, MNRAS, 406, 744

de Blok W. J. G., 2010, Advances in Astronomy, 2010

de Souza R. S., Mesinger A., Ferrara A., Haiman Z., Perna R., Yoshida N., 2013, MNRAS, 432, 3218

Deason A. J. et al., 2012, MNRAS, 425, 2840

Diemand J., Kuhlen M., Madau P., 2007, ApJ, 667, 859

Dodelson S., Widrow L. M., 1994, Physical Review Letters, 72, 17

Eke V. R., Cole S., Frenk C. S., 1996, MNRAS, 282, 263

Font A. S. et al., 2011, MNRAS, 417, 1260

Frenk C. S., White S. D. M., 2012, Annalen der Physik, 524, 507

Gao L., Theuns T., 2007, Science, 317, 1527

Gao L., Theuns T., Springel V., 2014, ArXiv e-prints

Gao L., White S. D. M., Jenkins A., Stoehr F., Springel V., 2004, MNRAS, 355, 819

Gorbunov D., Khmelnitsky A., Rubakov V., 2008, Journal of High Energy Physics, 12, 55

Guo Q., Cole S., Eke V., Frenk C., 2011, MNRAS, 417, 370

Guo Q., White S., Li C., Boylan-Kolchin M., 2010, MNRAS, 404, 1111

Ibata R., Martin N. F., Irwin M., Chapman S., Ferguson A. M. N., Lewis G. F., McConnachie A. W., 2007, ApJ, 671, 1591

Jenkins A., Frenk C. S., White S. D. M., Colberg J. M., Cole S., Evrard A. E., Couchman H. M. P., Yoshida N., 2001, MNRAS, 321, 372

Jiang L., Cole S., Sawala T., Frenk C. S., 2014, ArXiv e-prints

Kahn F. D., Woltjer L., 1959, ApJ, 130, 705

Kang X., Macciò A. V., Dutton A. A., 2013, ApJ, 767, 22

Komatsu E. et al., 2011, ApJS, 192, 18

Koposov S. et al., 2008, ApJ, 686, 279

Kusenko A., 2009, Phys. Rep., 481, 1

Lacey C., Cole S., 1993, MNRAS, 262, 627

Lagos C. d. P., Lacey C. G., Baugh C. M., 2013, arxiv:1303.6635

Lares M., Lambas D. G., Domínguez M. J., 2011, AJ, 142, 13

Li Y.-S., White S. D. M., 2008, MNRAS, 384, 1459

Libeskind N. I., Frenk C. S., Cole S., Helly J. C., Jenkins A., Navarro J. F., Power C., 2005, MNRAS, 363, 146

Liu L., Gerke B. F., Wechsler R. H., Behroozi P. S., Busha M. T., 2011, ApJ, 733, 62

Lovell M. R. et al., 2012, MNRAS, 420, 2318

Lovell M. R., Frenk C. S., Eke V. R., Jenkins A., Gao L., Theuns T., 2014, MNRAS, 439, 300

Lynden-Bell D., 1976, MNRAS, 174, 695

Lynden-Bell D., 1982, The Observatory, 102, 202

Macciò A. V., Fontanot F., 2010, MNRAS, 404, L16

Macciò A. V., Paduroiu S., Anderhalden D., Schneider A., Moore B., 2012, MNRAS, 424, 1105

Majewski S. R., 1994, ApJ, 431, L17

Martin N. F., Ibata R. A., Irwin M. J., Chapman S., Lewis G. F., Ferguson A. M. N., Tanvir N., McConnachie A. W., 2006, MNRAS, 371, 1983

Martin N. F. et al., 2009, ApJ, 705, 758

Martin N. F. et al., 2013, ApJ, 772, 15

McConnachie A. W. et al., 2009, Nature, 461, 66

Menci N., Fiore F., Lamastra A., 2012, MNRAS, 421, 2384

Miranda M., Macciò A. V., 2007, MNRAS, 382, 1225

Moroi T., Murayama H., Yamaguchi M., 1993, Physics Letters B, 303, 289

Narayanan V. K., Spergel D. N., Davé R., Ma C.-P., 2000, ApJ, 543, L103

Navarro J. F., Frenk C. S., White S. D. M., 1996, ApJ, 462, 563

Navarro J. F., Frenk C. S., White S. D. M., 1997, ApJ, 490, 493

Nierenberg A. M., Treu T., Menci N., Lu Y., Wang W., 2013, ApJ, 772, 146

Norberg P. et al., 2002, MNRAS, 336, 907

Okamoto T., Gao L., Theuns T., 2008, MNRAS, 390, 920

Pagels H., Primack J. R., 1982, Physical Review Letters, 48, 223

Pandolfi S., Evoli C., Ferrara A., Villaescusa-Navarro F., 2014, MNRAS, 442, 13

Parkinson H., Cole S., Helly J., 2008, MNRAS, 383, 557

Piffl T. et al., 2013, arxiv:1309.4293

Planck Collaboration et al., 2013, arxiv:1303.5062

Polisensky E., Ricotti M., 2011, Phys. Rev. D, 83, 043506

Pontzen A., Governato F., 2012, MNRAS, 421, 3464

Press W. H., Schechter P., 1974, ApJ, 187, 425

Purcell C. W., Zentner A. R., 2012, Journal of Cosmology and Astroparticle Physics, 12, 7

Rashkov V., Pillepich A., Deason A. J., Madau P., Rockosi C. M., Guedes J., Mayer L., 2013, ApJ, 773, L32

Schneider A., Smith R. E., Macciò A. V., Moore B., 2012, MNRAS, 424, 684

Schultz C., Oñorbe J., Abazajian K. N., Bullock J. S., 2014, MNRAS, 442, 1597

Shao S., Gao L., Theuns T., Frenk C. S., 2013, MNRAS, 430, 2346

Shi X., Fuller G. M., 1999, Physical Review Letters, 82, 2832

Smith R. E., Markovic K., 2011, Phys. Rev. D, 84, 063507

Somerville R. S., 2002, ApJ, 572, L23

Springel V. et al., 2008, MNRAS, 391, 1685

Strigari L. E., Wechsler R. H., 2012, ApJ, 749, 75

Tinker J., Kravtsov A. V., Klypin A., Abazajian K., Warren M., Yepes G., Gottlöber S., Holz D. E., 2008, ApJ, 688, 709

Tollerud E. J., Bullock J. S., Strigari L. E., Willman B., 2008, ApJ, 688, 277

Viel M., Becker G. D., Bolton J. S., Haehnelt M. G., 2013, Phys. Rev. D, 88, 043502

Viel M., Lesgourgues J., Haehnelt M. G., Matarrese S., Riotto A., 2005, Phys. Rev. D, 71, 063534

Wang J., Frenk C. S., Cooper A. P., 2013, MNRAS, 429, 1502

Wang J., Frenk C. S., Navarro J. F., Gao L., Sawala T., 2012, MNRAS, 424, 2715

Wang J., White S. D. M., 2007, MNRAS, 380, 93

Wang W., White S. D. M., 2012, MNRAS, 424, 2574

Weniger C., 2012, Journal of Cosmology and Astroparticle Physics, 8, 7

White S. D. M., Frenk C. S., Davis M., 1983, ApJ, 274, L1

Xu D. D., Sluse D., Gao L., Wang J., Frenk C., Mao S., Schneider P., 2013, arxiv:1307.4220

Xue X. X. et al., 2008, ApJ, 684, 1143

Yniguez B., Garrison-Kimmel S., Boylan-Kolchin M., Bullock J. S., 2014, MNRAS, 439, 73

Yoshida N., Sokasian A., Hernquist L., Springel V., 2003, ApJ, 591, L1

Zavala J., Vogelsberger M., Walker M. G., 2013, MNRAS, 431, L20